TRANSPORT AND POTENTIAL VORTICITY IN THE BAY OF BENGAL DURING THE SOUTHWEST MONSOON

V.S.N. Murty, C.S. Murty, Y.V.B. Sarma, D.P. Rao, J.S. Sastry, National Institute of Oceanography, Dona Paula, Goa - 403004, INDIA, and **G.R. Lakshamana Rao,** Department of Meteorology and Oceanography, Andhra University, Waltair - 503 003, INDIA.

ABSTRACT

In the Bay of Bengal, the water transport and potential vorticity (PV) during the southwest monsoon are examined through the prevailing thermohaline and wind-driven circulation. The Indian Monsoon Current (IMC) and the north flowing Eastern Boundary Current (EBC) contributed to an influx of 3.5 x 10^6 m^3/s and 5 x 10^6 m^3/s water respectively. The influence of overlying less saline, fresher water at the northern Bay; Ekman suction due to the wind stress curl in the central Bay; and the east-flowing IMC in the southern Bay have been explained in relation to distribution of PV on shallow (24.0 s_θ) isopycnal. The EBC is characterized by uniform, higher PV (100x10^{-11} $m^{-1}s^{-1}$) while the IMC by a lower value (75x10^{-11} $m^{-1}s^{-1}$). Following the depth of varying influence of wind from north (500 m) to the south (250 m), the waters of the Bay have been divided into upper and lower layers where horizontal advection and diffusion indicated dominance in the upper and lower layers up to 1200 m with predominant lateral (isopycnal) mixing over the vertical (cross-isopycnal) mixing.

INTRODUCTION

Of late, the increasing investigations to understand the dynamics of the circulation of the Bay of Bengal based on routine hydrographic data have revealed: a) the presence of gyral circulations (Varkey 1986, Murty 1990, Murty et al. 1992, 1993), b) meso-scale eddies (Swallow 1983, Babu et al. 1991), c) western boundary currents flowing poleward during April (Shetye et al. 1993) and Equatorward in November (Babu 1992), and d) thermohaline-driven poleward-flowing Eastern Boundary Current (EBC) west of the Andaman-Nicobar Islands during September to November (Murty et al. 1992, Suryanarayana et al. 1993). While the influence of freshwater influx as land and river run-off, wind forcing over the Bay, and the east- flowing Indian Monsoon Current (IMC) entering the Bay from the south on the circulation during the southwest monsoon has been documented (Murty 1990), the water characteristics, mixing, and near-surface circulation have been addressed by Murty et al. (1992). In this paper, the authors attempt to analyze the water transport and the potential vorticity (PV) distributions in the Bay of Bengal during the southwest monsoon, examined through the large-scale circulation and the mass balance within a meridionally oriented rectangular box.

DATA AND METHODOLOGY

DATA

The CTD data covering the Bay of Bengal during the southwest monsoon (August-September) presented by Murty et al. (1992) have been utilized for the present study. The data were collected along various zonal sections (Fig. 1) using the ME Sonde CTD system (accuracy:conductivity: +0.02 milli mho/cm, or salinity: + 0.002x10^{-3}; tem-

(1)

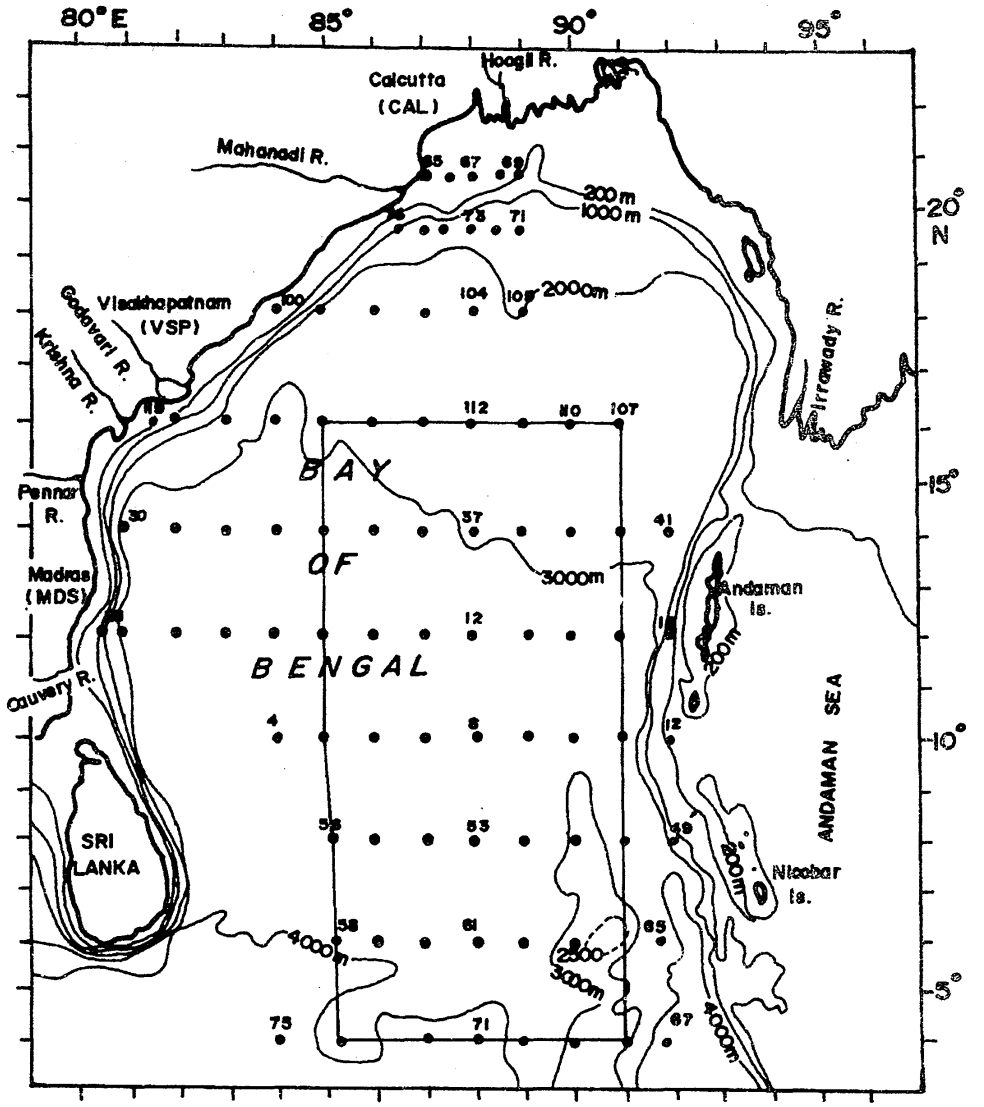

Figure 1: Map of the study area - Bay of Bengal, Showing the bathymetry and major rivers along its periphery. Hydrographic stations are shown a dots, and the numbers indicate the assigned serial station numbers. The rectangular area marked corresponds to Figure 10.

perature: + 0.01∞C; pressure: 0.5% of full range of 6000 dbar). The measured conductivity was converted into salinity in the CTD deck unit through practical salinity scale algorithms [Anon. 1981]. These values, at various pressure levels, were compared with those obtained through analysis of water samples using Autosal (Guildline make, Canada) collected at the same pressure levels using the CTD Rosette water samplers. Autosal values were higher than those of CTD at all the pressure levels, and the difference was inconsistent. After careful examination of the scatter plot (Fig. 2) between salinity values of CTD and Autosal, regression lines were fitted and the raw CTD data were corrected for all the stations. Salinity data, thus obtained are found to agree fairly well with that of the atlas

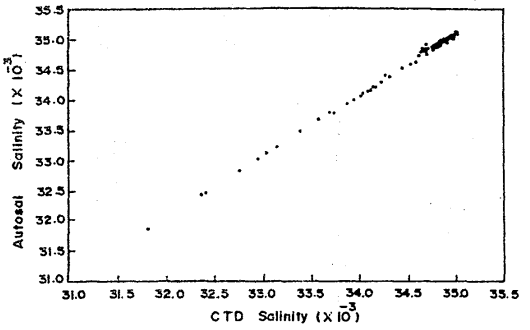

Figure 2: Scatter plot of CTD salinity versus Autosal salinity.

values. The spatial and temporal coverage achieved in this study exceed that of the data utilized in the atlases for this region (Wyrtki 1971, Levitus 1982). Below 26.0 δ_t, the differences in salinity compared to those of climatological sets are marginal (Fig. 3). Nonetheless, in the region north of 16°N lat. the signatures of freshening become conspicuous. The T-S plots displayed in Fig. 3 for the northern Bay (north of 15°N), the central Bay (15°-9°N), and the southern Bay (south of 9°N) along with the climatological data of Wyrtki (1971) show less scatter and more consistency below 25.0 6 (i.e. below 125 m depth). Above 25.0 δ_t, the wide scatter is evidently due to the penetration of Arabian Sea High Salinity Watermass (ASHSW) in the depth interval of 50 to 100 m (Sastry et al. 1985, Murty et al. 1992) and the influence of freshwater influx, confined to the top 90 m in the northern Bay and restricted to 50 m in the central Bay (Murty et al. 1992).

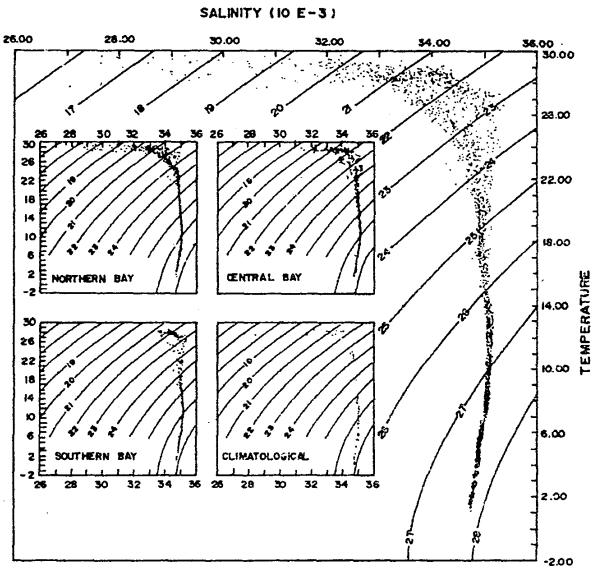

Figure 3: T-S plot for the Bay of Bengal during the southwest monsoon season of 1984. Region-wise T-S plots for the northern Bay (north of 15°N), the central Bay (between 15°N and 9°N), and the southern Bay (south of 9°N) together with the climatological T-S plot (Wyrtki 1971) are shown in the inset maps.

The sigma-t, potential temperature, potential density, specific volume anomaly, and the dynamic depth anomaly (_ D) at standard depths were computed through the NODC algorithms (Anon. 1974). For convenience, the depth of the water column in decibars is considered numerically equivalent to the depth in meters - an assumption having low impact on the computed transports.

ERROR ANALYSIS

The uncertainty in the dynamic height(s) mainly arise from the natural variability, measurement errors, apart from freely occurring low/high frequency wave motions. An error in the dynamic height, however small it might be, can adversely affect the computation of the (volume) transport. Inaccuracies in transport computations result from incorrect choices of level of no motion. In regions with strong velocity shear in the upper ocean and small

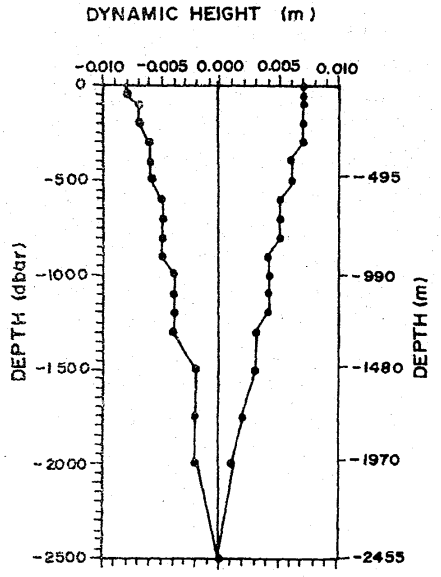

Figure 4: Vertical profiles of error in dynamic height (dyn.m.) obtained with the accuracy limits of a) T = + 0.01 °C & S = - 0.002 x 10^{-3}, and b) T = -0.01 °C & S = + 0.002 x 10^{-3}.

differences in the geopotential anomaly in the deeper sea, this error would be small (Stramma 1984).

In the present case, the fact that the observations pertain to a single survey lasting nearly 2 months, some degree of uncertainty in the computations of dynamic height(s) due to temporal variations in the temperature (T) and salinity (S) could not be avoided. For this reason, we compute the root-mean-square (rms) error in the dynamic height(s) due to measurement errors in T and S. The mean standard deviation of dynamic height at 500 m, 1000 m, and 1500 m relative to 2500 dbar is 1.53, 0.91, and 0.64 dyn.cm. respectively along the latitudinal sections, while along the meridional sections (85°E and 91°E) the respective standard deviations are 4, 3, and 2 dyn.cm. Using the data on T and S at 10 dbar interval at one station (4°N, 87°E) the computed variation of dynamic height (Fig. 4), within the accuracy limits of T and S, shows a variation of 1.5 dyn.cm. at the sea surface which decreases to 0.3 dyn.cm. at 2000 dbar. Here, the estimated rms error in dynamic height is 1.0 dyn.cm. From the above, the rms error in the (volume) transport at 4°N works out to 1.01 x 10^6 m^3/s - corresponding to an error percentage of <3 over the total transport. With increasing latitude, while the rms error shows a decrease to 0.25 x 10^6 m^3/s at 16°N the error percentage over the total transport remained constant. This error is far less, compared to errors estimated by Stramma (1984) for the eastern subtropical northern Atlantic.

METHODOLOGY

The volume (mass) transport is computed (Sverdrup et al. 1942) with three reference level surfaces (500, 1000; and 2500 dbar) to examine the variations in the transport. For stations with depths shallower than those of reference surfaces, the specific volume anomaly has been extrapolated following Fomin (1964). While there is an unresolved debate on the choice of the depth of "reference level surface" (Stramma 1984), basically the selection depends on the availability of data at as many levels as possible within the water column. For this area of study, 500 dbar surface was used, following Defant's method (Varadachari et al. 1968); and 2500 dbar surface was suggested based on the vertical profiles of mean and variance of differences of mean specific volume anomaly (Varkey and Sastry 1988). The existence of intermediate layer (1200-1700 m) with dominating horizontal flows (Bennett 1970, Varkey 1986) rules out the selection of reference level in this depth zone. Further, the studies of Sewell (1932), Gallaghar (1966), Bennett (1970), and Wyrtki (1971) indicate the penetration of north Indian Ocean Deep Watermass (characterized by higher oxygen 3.17-4.17 ml/l; S=34.68-34.78x10^{-3}; and T=1.6-2.8°C) and Indian Ocean Bottom Watermass

(O_2=4.03-4.68 ml/l; S=34.69-34.77x10^{-3}; T=0.2-1.47°C) extending to the head of the Bay, at depths greater than 1500 m. Considering 2500 m as the lower depth limit of this northward-moving deep water (upward from 2500-1700 m), vertical motions could dominate horizontal motions at these depths. This suggests that 2500 dbar surface could be chosen as the level of no motion for the Bay of Bengal. As the study area is subjected to seasonal variability, we consider 1000 dbar as the intermediate reference level and 500 dbar as the upper reference level besides 2500 dbar, for volume (mass) transport computations.

The mass transport computations, assuming mean geostrophic flow to prevail between station pairs, have been made with reference to 2500 dbar surface for the volume of water between lat. 4°N-16°N and long. 85°E-91°E covering depths up to 2500 dbar. Utilizing the 2° x 2° grids (chosen to overcome inhomogeneity in the hydrographic station coverage), the net volume transports are estimated.

The distribution of potential vorticity (PV) is examined as an indicator of large-scale circulation neglecting the relative vorticity. While McCartney (1982) and Talley (1988) utilized the density gradient (∂_/∂Z) and Coriolis parameter ("f") to obtain potential vorticity ("q") defined as

$$q = (f/\_)\partial\_/\partial Z \qquad (1)$$

in the present study, this relation, in finite difference form, similar to that of McDowell et al. (1982)

$$q = g\, f\, \_s_Q/\_P \qquad (2)$$

has been used. Here, "g" is the acceleration due to gravity (980 cm/s^2), "f" is the Coriolis parameter (2w Sin Q, w is the angular velocity of earth (7.29x10^{-5} radians/s) and F

Isopycnal Layer				
From	To σ_o	Mean	Depth (dbar)	
			From	To
23.5	24.0	23.8	50	120
25.0	25.2	25.1	100	165
26.0	26.2	26.1	150	230
26.4	26.6	26.5	180	300
26.8	27.0	26.9	330	450
27.0	27.2	27.1	480	610
27.2	27.4	27.3	680	840
27.4	27.6	27.5	865	1340
36.75	37.0	36.8	1660	2025

Table 1: Isopycnal layers - their limits.

is latitude), _P is thickness of the isopycnal layer (or distance between the isopycnal surfaces) in decibars, and s_Q is potential density (in parts per thousand; g/cm^3) of the isopycnal

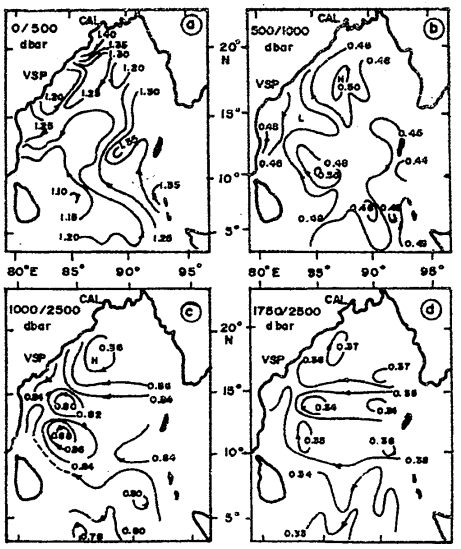

Figure 5: Maps of dynamic topography (dyn.m.) at different depths: a) 0/500 dbar, b) 500/1000 dbar, c) 1000/2500 dbar, and d) 1750/2500 dbar (after Murty 1990).

surface with reference to sea surface pressure (0 dbar). The PV is computed for various isopycnal layers (Table 1). Reckoning the potential density w.r.t. to 2000 dbar following Reid and Lynn (1971), the PV on the 36.8 s_2 surface is computed.

The zonal averaging of PV is done as it reduces the noise in the distribution maps on the isopycnal layers. For each isopycnal the oceanic rest state PV is obtained at each latitude by multiplying the mean value of $(g\Delta\delta_s/\Delta P)$ for the isopycnal with "f".

RESULTS

The studies of Murty (1990) and Murty et al. (1992) on the circulation (Fig. 5a to d) and water characteristics documented the presence of a large cyclonic gyre south of 15°N encompassing the ASHSW in the depth range of 50-100 m, and anticyclonic, cellular flows on the east and north of the above apart from a general westward flow at 14°N-15°N. In addition, these studies also reported differential flows at 500 m, 1000 m, and 1750 m depths.

TRANSPORT

The geostrophic volume transport in the upper 500, 1000, and 2500 m across 12°N presents asymmetric (Fig. 6a and 6b) and alternating (Fig. 6c) trend. Below 500 m, west of 85°E, the northward and southward transports result from the anticyclonic circulation (Fig. 5b to 5d). Relative to the three reference surfaces, the computed transport in the top 100 m shows an influx (2.3×10^6 m^3/s) excluding the southward-directed Ekman transport of 2.5×10^6 m^3/s (Murty et al. 1993). In the upper 500 m (Fig. 6a), the transport shows very low influx while in the upper 1000 m (Fig. 6b) weak outflux prevails. Over the 2500 column (Fig. 6c), the transport shows an influx of nearly 6×10^6 m^3/s. This suggests weak outflux between 500 m and 1000 m with an influx (northward flow) below 1000 m in the western Bay.

Across the zonal sections, in the upper 2500 m (Fig. 7), a southward transport of 14, 9, and 15×10^6 m^3/s is noticed across 16°N, 14°N, and 12°N respectively close to the western boundary. The pattern of transports along

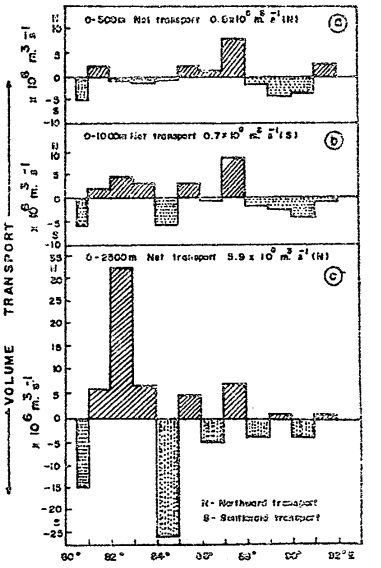

Figure 6: Volume transport (x106 m3/s) across 12°N section for the water column above each of the reference level a) 500 dbar, b) 1000 dbar, and c) 2500 dbar. (Hatching/stippling indicates northward [N]/southward [S] transport).

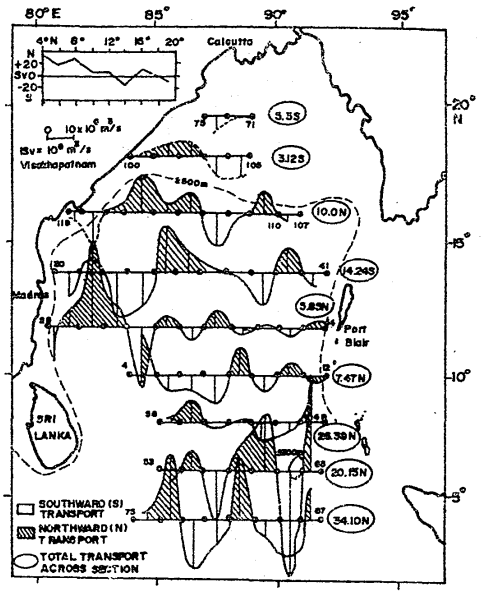

Figure 7: Volume transport (x 106 m3/s) in the upper 2500 m across the zonal sections. The broken line indicates the 2500 m isobath. The transports computed through extrapolation method are shown by broken curves (inside the 2500 m isobath). The inset indicates the total transport against latitude.

The gridwise transports show higher net transports in the southern Bay (Fig. 9). The number in the ellipse of each grid gives the surplus/deficit while reckoning the geostrophic balance. The net transports are negative (deficit) west of 88°E and south of 12°N. North of 8°N lat., the surplus (positive) and deficit transports vary from 0.2 x 10^6 m^3/s to 2.0 x 10^6 m^3/s and lead to an overall weak, net divergence of 0.7 x 10^6 m^3/s, which is close to the error limits estimated for transport computation. The low values mean minimum frictional effects and contribute to the balance from quasi-geostrophy (Febres-Ortega and Herrera 1976). The large surplus and deficit net transports in the southern Bay (south of 8°N) are due to the effect of north-south meandering in the westward flow at deeper depths and due to the effect of diminishing "f". Here the possible influences of remote forcing from low-frequency Rossby waves cannot be ignored.

4°N and 6°N reflect the north-south meandering flow at deeper depths (Fig. 5c). Higher magnitudes result from lower values of "f" and are possibly influenced remotely by low-frequency Rossby waves.

The transport in the upper 100 m (Fig. 8) relative to 2500 dbar is similar to that for the water column of 2500 m (Fig. 7). Murty et al. (1992) identified strong (40 cm/s) northward-flowing current in the upper 100 m across 6°N between 90°30'E and 91°50'E. This has been named as the Eastern Boundary Current. This current, constituting waters of the Andaman Sea with salinity <34.4 x 10^{-3}, transports about 5 x 10^6 m^3/s of water toward north across 4°, 6°, and 8°N. West of 90°30'E, the transport (contrastingly characterized by higher salinities 34.5-35.0x10^{-3}) is directed northward with a mean value of 3.5 x 10^6 m^3/s, indicating influx associated with IMC.

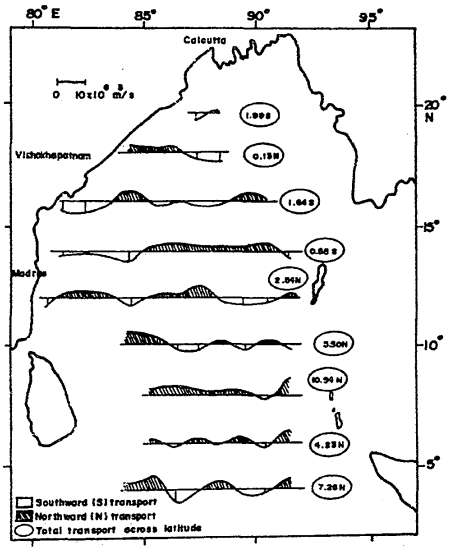

Figure 8: Same as in Figure 7, but for the top 100 m water column.

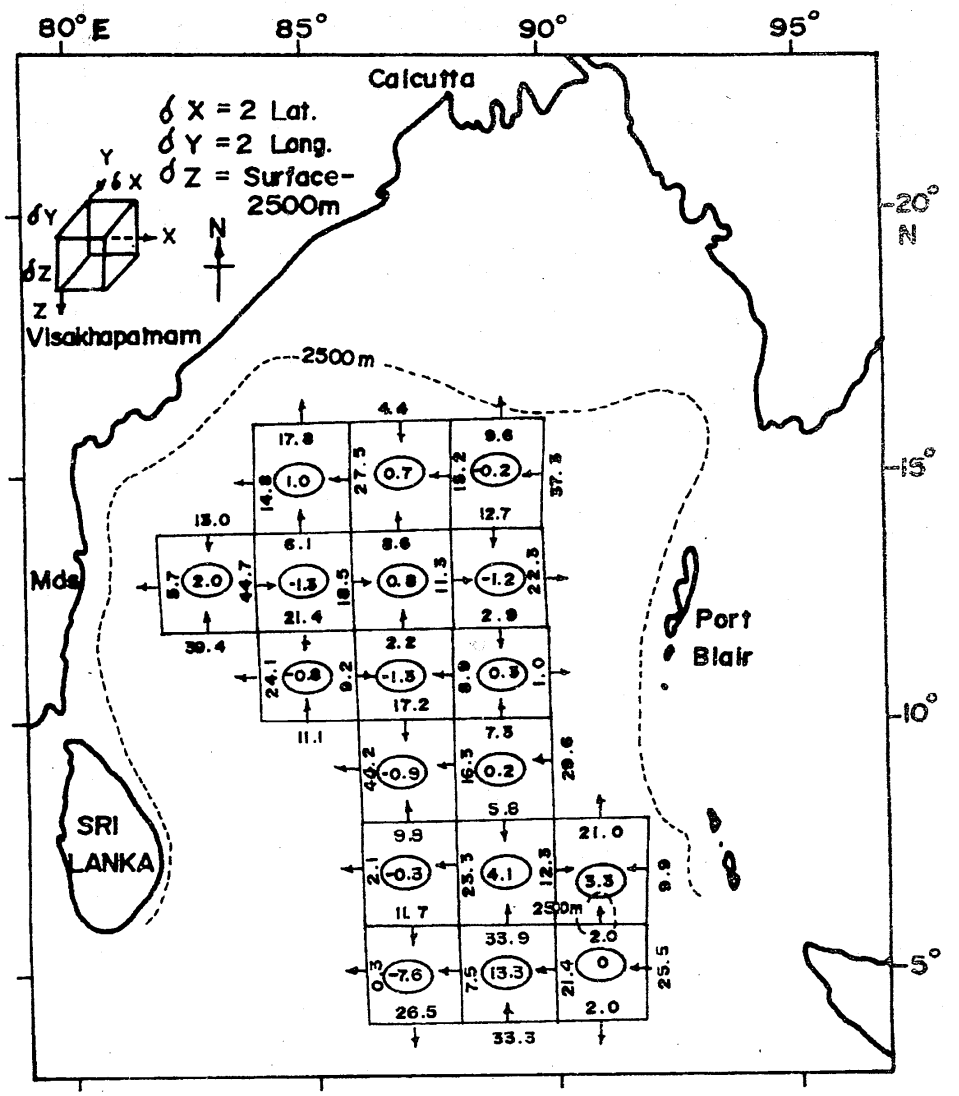

Figure 9: Net volume transports (x 106 m3/s) in 2° x 2° grids of the study area. The numbers in the ellipses indicate the surplus (positive) and deficit (negative) transports while reckoning for the geostrophic balance.

The transports across the side walls of the rectangular box are directed toward north and west (Fig. 10). On the southern and western sides the magnitudes are large. Within the box, the mass transports (Table 2) indicate convergence (surplus) in Layer 1 and divergence (deficit) in Layers 2 to 4, followed by weak convergence in Layers 5 and 6. Except in Layer 2, both the surplus and deficit transports in the layers result from the higher net mass convergence and divergence respectively due to zonal transports. These surplus and deficit transports give rise to vertical flows across the bottom of each layer. This means that the

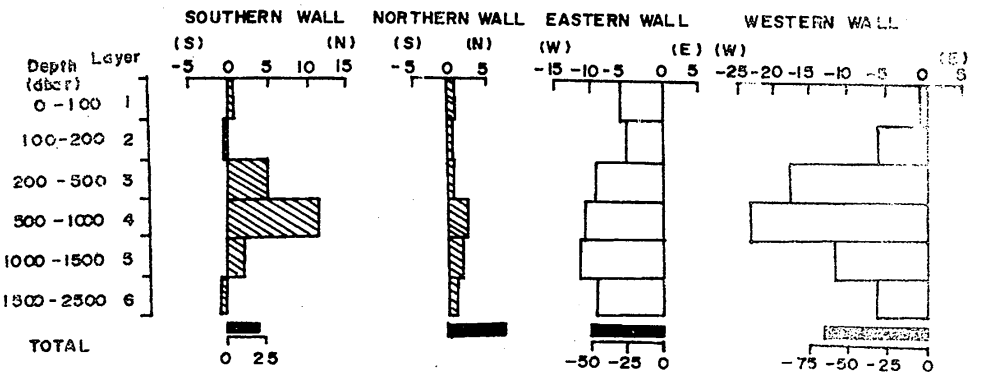

Figure 10: Layerwise volume transport (x106 m3/s) in the upper 2500 m across the sides of the rectangular box. (N/S: northward/southward transport; E/W: eastward/westward transport). Note the change of scale for total transports across the side walls.

Layer	Depth (dbar)	South wall		North wall		Net_M	West wall		East wall		Net_Z	Net_B
		N	S	N	S		W	E	W	E		
1	0 - 100	8.53	7.92	3.94	3.00	-0.33	13.12	10.67	10.20	4.29	3.46	3.13
2	100 - 200	5.88	6.14	2.06	1.81	-0.51	13.58	7.39	8.39	2.89	-0.70	-1.21
3	200 - 500	15.36	10.44	5.63	4.55	3.83	32.49	15.96	19.05	9.55	-7.01	-3.20
4	500 - 1000	20.32	8.66	6.94	5.04	9.77	37.99	15.50	23.21	11.74	-11.02	-1.25
5	1000 - 1500	9.39	7.56	3.87	1.82	-0.22	19.97	8.23	17.28	5.28	0.26	0.04
6	1500 - 2500	5.69	6.40	2.55	1.08	-2.18	12.99	5.93	14.17	4.53	2.58	0.40
Total		65.17	47.12	24.99	17.30	10.36	130.14	63.68	92.29	38.28	-12.45	-2.09

Table 2: Mass transport ($x10^9$ kg/s) in each layer for the upper 2500 m. N/S: transport toward north/south; W/E: transport toward west/east. Negative numbers indicate net mass divergence due to meridional (Net_M) and zonal (Net_Z) transports and within the layer of the box (Net_B).

surplus transport of 3.13 x 10^9 kg/s in Layer 1 should give rise to a downward transport at the layer interface at 100 m. This input overcompensates the computed deficit of 1.21 x 10^9 kg/s in Layer 2 and contributes further down to Layer 3 at a depth of 200 m. This downward transport (1.92x10^9 kg/s) partly compensates the deficit of 3.2 x 10^9 kg/s in Layer 3. For a perfect balance, an upward transport of 1.28 x 10^9 kg/s through the bottom of Layer 3 (i.e. at 500 m) becomes essential. Thus, together with this and the deficit of 1.25 x 10^9 kg/s in Layer 4, the upward transport should be 2.53 x 10^9 kg/s from a depth of 1000 m. The observed weak mass convergence in Layers 5 and 6 is close to the transport error and is suggestive of a mass balance below 1000 m.

POTENTIAL VORTICITY

The distribution of PV is examined along a meridional section and on select isopycnal surfaces. The meridional distribution of PV in the vertical along 88°E (Fig. 11) shows a maximum value varying between 1500 and 2000 x 10^{-11} $m^{-1}s^{-1}$ in the upper 10 m north of 16°N and a rapid decrease over a depth of 60 m (hatched portion). Between 16°N and 14°N, strong horizontal gradients of PV prevail at the sea surface. South of 14°N, the near-surface isostrophs (lines of equal "q") and the subsurface PV maximum (shown by thick arrow) deepen southward. Below a depth of 100 m the isostrophs are inclined toward north in general from 4°N up to 12°N, and further northward the isostrophs labelled 40, 30, 20,and

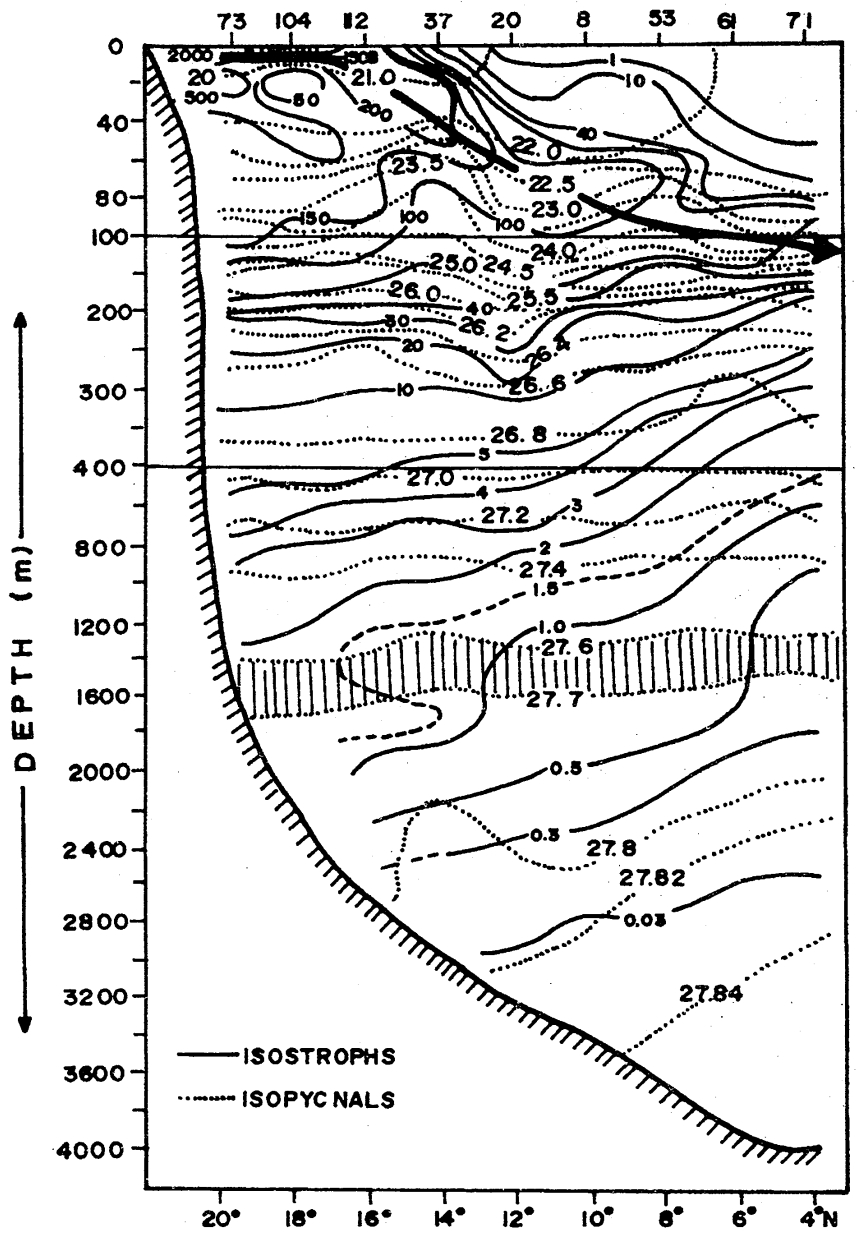

Figure 11: Meridional distribution of PV (x10-11 m-1s-1) along 88°E section. (Layer of uniform PV is hatched. Arrow indicates axis of PV maximum).

10 tend to lie nearly horizontal between 200 and 300 m and also parallel to the isopycnals (dotted lines) from 26.0 to 26.7 s_Q. In the depth range of 300-1400 m the isostrophs labelled 5, 4, 3, and 2 make steep angles with isopycnals lying horizontal from south to north while the isostrophs in the depth interval 1400-1700 m are nearly normal to the isopycnals 27.6 and 27.7 s_Q (hatched zone). Below 1700 m the isopycnals and isostrophs are parallel to each other.

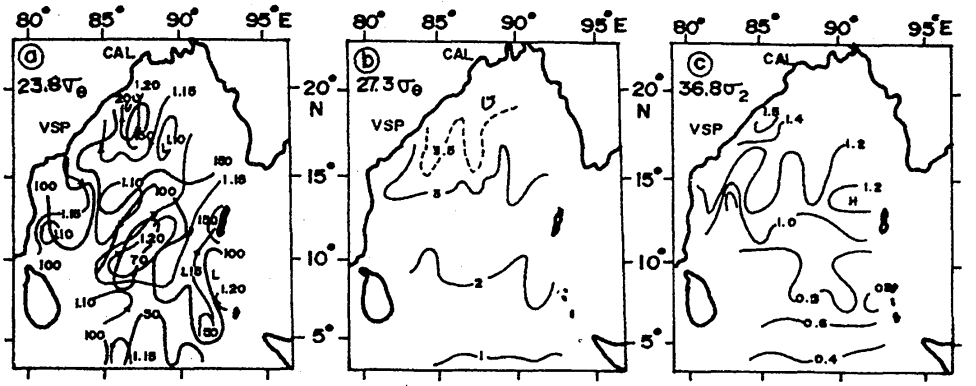

Figure 12: Meridional variation of zonal average of PV (thick lines) and oceanic rest state PV (thin lines) for various isopycnals. Note the change in the scale of ordinate.

The distribution of PV on shallow (23.8 s_Q), intermediate (27.3 s_Q), and deeper (36.8 s_2) isopycnals (Fig. 12a to c) could broadly be summarized as: a) on 23.8 s_Q surface, higher (150-200x10^{-11} $m^{-1}s^{-1}$) values of PV occurred in the northern Bay with lower (50x$10^{-11}m^{-1}$ s^{-1}) values in the southern Bay (Fig. 12a); b) on 27.3 s_Q surface, PV increased gradually northward and the isostrophs are aligned zonally except in the western Bay and north of 15°N (Fig. 12b); and c) on 36.8 s_2 surface, PV exhibits uniform value between 6∞N and 10°N though the distribution is somewhat noisy toward north (Fig. 12c).

The zonal average of PV is slightly less from the oceanic rest state PV north of 8°N on shallower isopycnals between 23.8 and 25.1 s_Q (Fig. 13) and north of 14°N on the deeper isopycnals greater than 25.1 s_Q. If the zonal average of PV is parallel to the smooth "ß"-curve, the meridional gradient of PV is proportional to ß. Along 23.8 s_Q, the gradient is >between 4°N and 6°N and <between 16°N and 18°N. On 25.1 s_Q surface the PV is dominated by "f" over a large area between 8°N and 16°N, and its meridional gradient is "ß". Dominance of "f" extends to 6°N on 26.1 s_Q and from 4°N to 18°N on deeper (27.1, 27.3 s_Q and 36.8 s_2) isopy.

DISCUSSION

From the estimated net fluxes of transports across 12°N, one identifies a northward transport in the top 500 m, a southward transport between 500 and 1000 m, and a northward transport below 1000 m. The deep, northward flow leads to upward vertical flows from deeper depths. This is so for Bay of Bengal with its northern boundary closed and when one examines through the abyssal circulation model of Stommel and Arons (1960). Such a vertical flow at depths of 2300 m is also reported for this marginal sea (Bennett 1970). The observed net mass divergence within the rectangular box requiring an upward transport from 1000 m could be achieved from the vertical flows associated with the northward penetration of deep and bottom watermasses at these depths or largely to be compensated in the form of mass convergence elsewhere or outside the domain of this box. The flows (transports) directed toward the western Bay support this conjecture of large-scale convergence followed by sinking. Supporting evidence could be seen from the southward-directed strong surface currents in the western and southwestern Bay during August and September (Cutler and Swallow 1984).

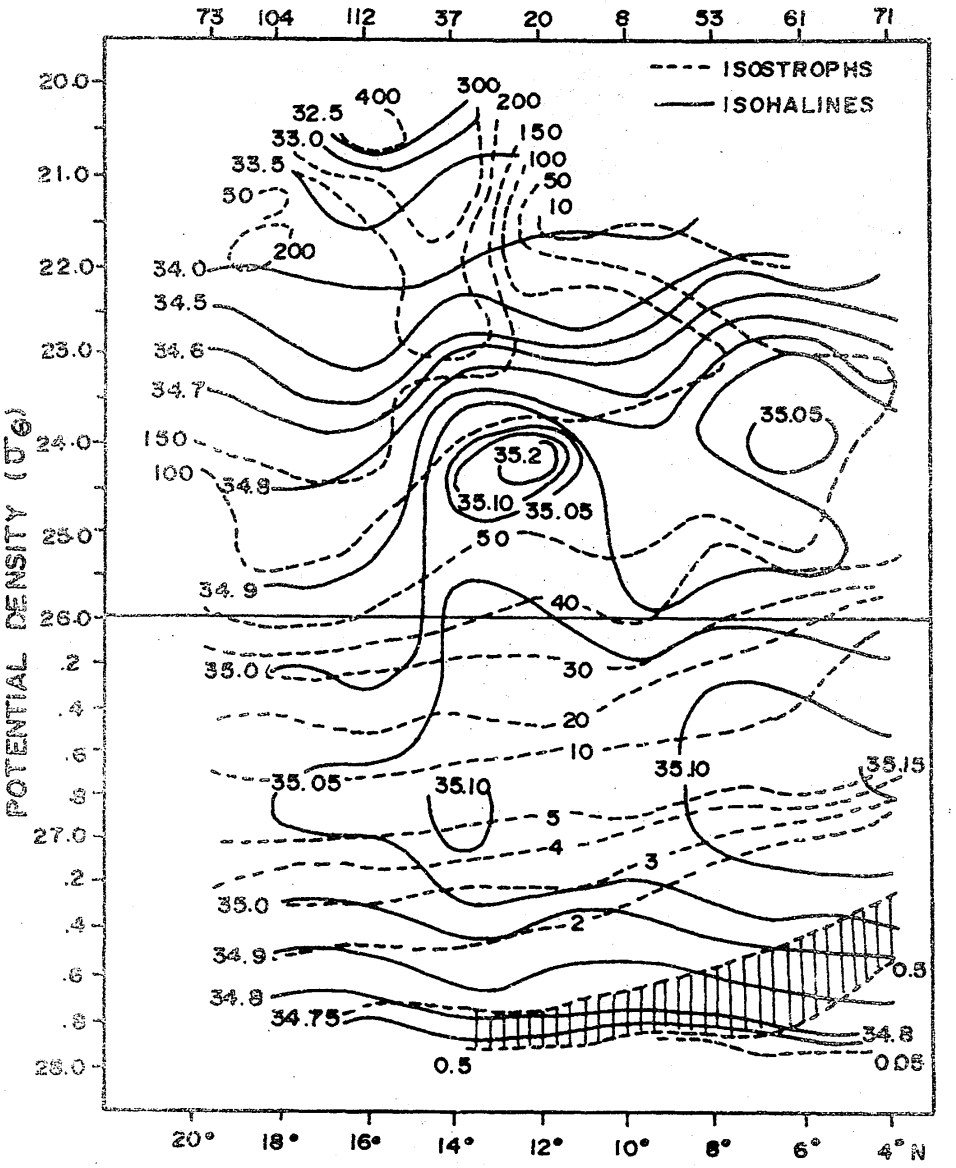

Figure 13: Distribution of PV (x10-11 m-1s-1) on a) 23.8sQ with superimposed dynamic topography at 100/1000 dbar, b) 27.3 sQ, c) 36.8 s2 isopycnals.

The observed higher PV in the north Bay (Fig. 11) results from the prevailing shallow halocline developed due to overlying dilute waters and the associated vertical density structure (Sastry et al. 1985, Murty et al. 1992). In the central Bay the influence of freshwater reaches only to depths of 40 m with the field of vertical velocity, beneath the surface Ekman layer, showing higher, positive values (Ekman suction). Under its influence the isostrophs from the south rise toward the sea surface. The lower values of PV in the southern Bay are due to weak vertical density gradients associated with a large homogeneous surface layer. The northward increase of "q" on 23.8 s_Q surface (Fig. 12a) is slightly less than the north-

ward increase of "f" (nearly five times), and the distribution of "q" exhibits similarity to the circulation at 100 m (falling within the depth domain of this isopycnal; Table 1). The low "q" in the central Bay is associated with the anticyclonic circulation. Though IMC is less distinguishable at this depth in the southern Bay, PV varies between 100 and 50 x 10^{-11} $m^{-1}s^{-1}$. East of 91°E, the EBC is characterized by uniform PV ($100x10^{-11}$ $m^{-1}s^{-1}$) in contrast to higher values ($150\ x10^{-11}m^{-1}s^{-1}$) west of it.

Within the intermediate depths and isopycnals (Fig. 11 and 12b), the PV distribution is dominated by "f." The weak lateral and meridional gradients of PV with the zonal isostrophs suggest that the flow is weak (closer to "rest state") and mostly zonal (Fig. 5c). This only means that the strong forcing at the sea surface does not effect these isopycnals which are greater than 27.1 s_Q. Young and Rhines (1982) also predict PV dominated by "f" with weak wind forcing. Keffer (1985) also reported zonally oriented isostrophs at these isopycnals for the present area of study. Thus, the depth of influence of the wind forcing could best be delineated through PV distribution which helps separation of the waters of the Bay above 27.0 s_Q isopycnal from those below. In the south Bay, the "" effect is noticed on 26.5 s_Q isopycnal and underlines the influence of surface wind forcing. This demonstrates that the depth of influence of wind forcing is limited to the upper 250 m (26.5 s_Q) in the south Bay and to 500 m (27.0 s_Q) in the north Bay (Fig. 11) - demarcated by the isostroph 5 x 10^{-11} $m^{-1}s^{-1}$. In the Equatorial regions of the Bay, though the wind field is strong and prevails longer (June through September), its influence reaches only to shallow depths - an observation documented also by Shcherbinin (1978) during the southwest monsoon in the southern Bay.

Below the depth of wind influence, the circulation must be due to thermohaline forcing or strongly controlled by diffusion processes. For this area of study, earlier researchers (Bennett 1970) identified uniform vertical diffusive flux from 400 to 1200 m and uniform vertical advection at deeper depths below 1700 m with a transition between 1200 and 1700 m. This transition zone coincides with the transition layer with nearly uniform PV in which

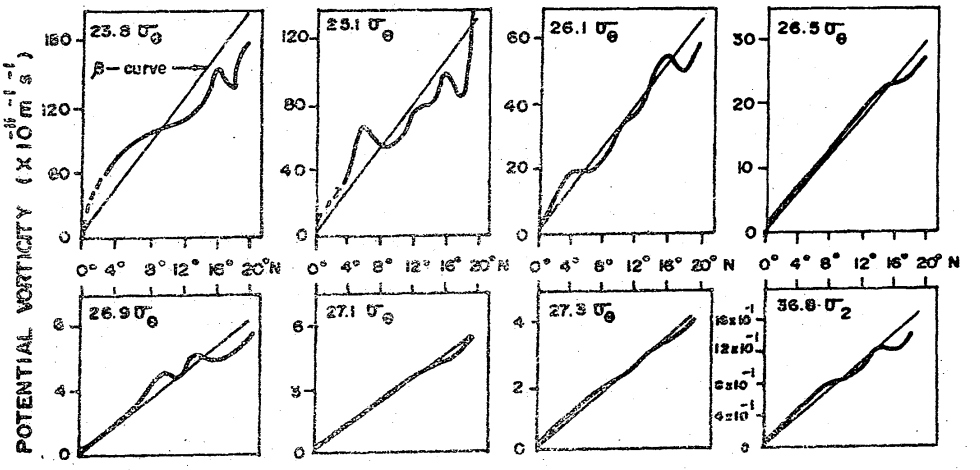

Figure 14: Meridional distribution of salinity (x10-3) and PV along 8E section with potential density (sQ) as ordinate.

the isostrophs are orthogonal to the isopycnals (Fig. 11). Bennett (1970) opines that in the diffusive flux zone contraction of volume (or densification) during mixing is the main mechanism and there is a net southward mass flux from the layer 400-1200 m. To compensate this mass outflux, there should be a net mass ascent from the deeper depths associated with the northward penetration of deep watermass up to the head of the Bay.

In order to ascertain the influence of diffusion and the advection in the upper and lower layers, the distribution of two tracer parameters - PV and salinity - along 88°E section (Fig. 14) has been examined. The salinity distribution identifies the low salinity waters at 16°N, two high salinity pockets (>35.05x10^{-3}) centred at 6°N and 12°N in association with the advection of ASHSW between 23.5 and 24.0 s_Q isopycnals, and the presence of an isohaline (>35.05x10^{-3}) layer with its salinity and thickness decreasing northward between 26.2 and 27.3 s_Q isopycnals. The isohalines and isostrophs exhibit parallelism below 24.0 s_Q north of 15°N. Elsewhere, one would see large vertical excursions of isostrophs and isohalines across the isopycnals above 25.0 s_Q between 16°N and 12°N, and also both the isolines making steep angles with the shallower (<25.0 s_Q) isopycnals south of 12°N and deeper (>25.0 s_Q) isopycnals south of 15°N. This feature is suggestive of dominant mixing in conformity with the studies of Roemmich and Wunsch (1985). Following density flux function in conjunction with density, Murty et al. (1992) inferred vertical mixing at the region of vertical excursions (above 25.0 s_Q) associated with the high salinity pockets and lateral mixing in the region where the isohalines and isostrophs are making steep angles with the isopycnals.

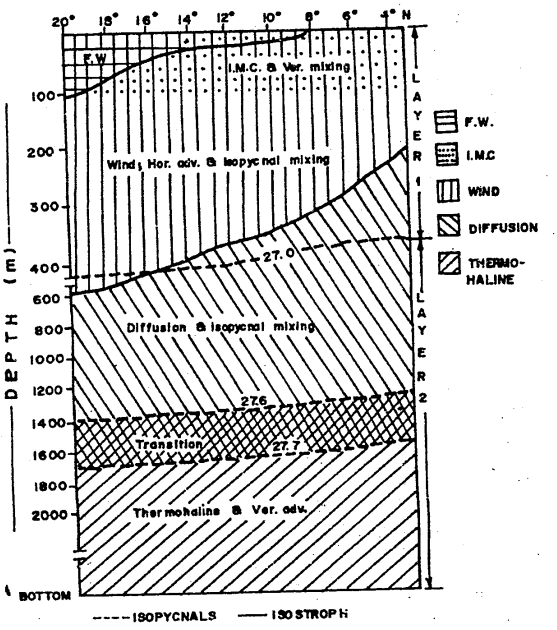

Figure 15: Sketch of the depth limits of influence of freshwater influx (FW), Indian Monsoon Current (IMC), and wind forcing together with the dominant processes operating in the upper and lower layers of the Bay of Bengal during the southwest monsoon.

Thus, in the upper 400 m (<27.0 s_Q isopycnal) the horizontal advection influences the property distributions as the circulation is influenced by the dominant wind forcing and by the buoyancy forcing from freshwater influx in the northern and eastern Bay. Below this layer (>27.0 s_Q isopycnal), vertical diffusion of density dominates the circulation from 400 to 1200 m. Below 1200 m, thermohaline forcing with vertical advection at depths greater than 1700 m associated with the movement of the deep watermass becomes important. Here, the geostrophic circulation shows northwestward flow up to the Indian coast. Lateral mixing is predominant in the upper and lower layers. The depth limits of freshwater influx, the IMC, and the wind forcing together with the various dominant processes identified in the domains of the upper and lower layers of the Bay are schematically shown in Fig. 15.

CONCLUSIONS

The pattern of geostrophic transport relative to 500 dbar and 1000 dbar reference levels does not exhibit appreciable variations, while the changes in the magnitude and pattern of transport become significant for the 2500 dbar reference level. The IMC and the EBC (100 km wide) transport about 3.5 x 10^6 m^3/s and 5 x 10^6 m^3/s of water toward north in the upper 100 m respectively.

Analysis of PV distribution reveals the dominance of "f" ("ß"-effect) on the isopycnals deeper than 27.0 s_θ. This enables separation of the Bay waters into the upper (above 400 m depth) and lower (below 400 m depth) layers in contrast to three regions from the property distributions (Murty et al. 1992). The influence of freshwater influx in the northern Bay on shallower isopycnals and wind forcing reaching depths of 250 m in the southern and 500 m in the northern Bay have been clearly demarcated. The narrow EBC is characterized by uniform and higher values of PV of 100 x $10^{-11}m^{-1}s^{-1}$ as against lower values associated with the IMC. Horizontal advection is dominant in the upper layer. In the lower layer, diffusion controls the circulation of water between 400 and 1200 m while thermohaline forcing becomes important below depths of 1200 m. Lateral mixing is predominant in both the layers.

ACKNOWLEDGEMENTS

The authors express their gratitude to Dr. E. Desa (Director) and Dr. B.N. Desai (former Director), N.I.O., for their keen interest in this study.

REFERENCES

Anon. (1974). Key to oceanographic records documentation No. 1, User's guide to NODC's Data Services (revised). NODC, Washington, D.C.

Anon. (1981). UNESCO technical papers in Marine Sciences. Rep. 37: 144 p.

Babu, M.T., Kumar, S.P. and Rao, D.P. (1991). A subsurface cyclonic eddy in the Bay of Bengal. J. Mar. Res., 49: 403-410

Babu, M.T. (1992). Equatorward western boundary current in the Bay of Bengal during November-December, 1983, p. 57-62. In G.N. Swamy, M.K. Antony, and V. Kesava Das (ed.). Physical Processes in the Indian Seas (Proceedings of the First Convention of the Indian Society of the Physical Sciences of the Ocean. Published by ISPSO, Goa, 57-62.

Bennett, E.B. (1970). Turbulent diffusion, advection and water structure in the North Indian Ocean. Ph.D. Dissertation (unpubl.). University of Hawaii, Honolulu, 133 p.

Cutler, A.N. and Swallow, J.C. (1984). Surface currents of the Indian Ocean (to 25°S, 100°E): Compiled from historical data archived by Meteorological Office, Bracknell, U.K. International Oceanographic Sciences, Rep. 187: 8 p., 36 charts.

Febres-Ortega, G. and Herrera, L.E. (1964). Caribbean Sea circulation and water transports near the Lesser Antilles. Bol. Inst. Oceanogr., University of Oriente, 15: 83-96.

Fomin, L.M. (1964). The Dynamic Method in Oceanography, Elsevier Publ. Co., Amsterdam, 212 p.

Gallaghar, J.F. (1966). The variability of watermasses in the Indian Ocean. NODC General Series, Publ. G-11, U.S. Naval Oceanogr. Office, Washington, D.C., 74 p.

Keffer, T. (1985). The ventilation of the world's oceans: Maps of potential vorticity field. J. Phys. Oceanogr. 15: 509-523.

Levitus, S. (1982). Climatological atlas of the world ocean. NOAA Professional Paper 13: U.S. Govt. Printing Office, 173 p.

McCartney, M.S. (1982). The subtropical recirculation of mode waters. J. Mar. Res. 40(Suppl.): 427-464.

McDowell, S., Rhines, S. and Keffer, T. (1982). North Atlantic potential vorticity and its relation to general circulation. J. Phys. Oceanogr. 12: 1417-1436.

Murty, V.S.N. (1990). Some aspects of large scale circulation in the Bay of Bengal during south west monsoon. Ph.D thesis (unpubl.), Andhra University, Waltair, India, 141 p.

Murty, V.S.N., Sarma, Y.V.B. Rao, D.P. and Murty, C.S. (1992). Water characteristics, mixing and circulation in the Bay of Bengal during southwest monsoon. J. Mar. Res. 50: 207-228.

Murty, V.S.N., Suryanarayana, A. and Rao, D.P. (1993). Current structure and volume transport across 12∞N in the Bay of Bengal. Indian J. Mar. Sci. 22: 12-16.

Reid, J.L., and Lynn, J. (1971). On the influence of the Norwegian Greenland and Weddell Seas upon the bottom of the Indian and Pacific Oceans. Deep-Sea Res. 18: 1063-1088.

Roemmich, D., and Wunsch, C. (1985). Two transatlantic sections: Meridional circulation and heat flux in the subtropical North Atlantic Ocean. Deep-Sea Res. 6: 619-664.

Sastry, J.S., Rao, D.P. Murty, V.S.N. Sarma, Y.V.B. Suryanarayana, A. and Babu, M.T. (1985). Watermass structure in the Bay of Bengal. Mahasagar-Bull. Natl. Inst. Oceanogr. 18: 155-162.

Sewell, R.B.S. (1932). Geographic and oceanographic research in Indian waters: Temperature and salinity of the deep waters of the Bay of Bengal and Andaman Sea. Memoirs of Asiatic Society of Bengal, 9(6): 357-423.

Shcherbinin, A.D. (1978). Geostrophic water circulation in the Indian Ocean. Oceanology, 13: 649-654.

Shetye, S.R., Gouveia, A.D. Shenoi, S.S.C. Sunder, D. Michael, G.S. and Nampoothiri, G. (1993). The western boundary current of the seasonal subtropical gyre in the Bay of Bengal. J.Geophys. Res. 98(C1): 945-954.

Stommel, H., and Arons, A.B. (1960). On the abyssal circulation of the world's ocean. I. Stationary planetary flow patterns on a sphere. Deep-Sea Res. 6: 140-154.

Stramma, L. (1984). Geostrophic transport in the warm water sphere of the eastern subtropical North Atlantic. J. Mar. Res. 42: 537-558.

Suryanarayana, A., Murty, V.S.N. and Rao, D.P. (1993). Hydrography and circulation in the Bay of Bengal during late winter, 1983. Deep-Sea Res. I,40: 205-217.

Sverdrup, H.U., Johnson,M.W. and Fleming, F.R. (1942). The Oceans: Their Physics, Chemistry and General biology. Prentice-Hall, New-York, 1087 p.

Swallow, J.C. (1983). Eddies in the Indian Ocean. In A. Robinson (ed.). Eddies in Marine Sciences. Springer-Verlag, New York, 609 p.

Talley, L.D. (1988). The potential vorticity distribution in the north Pacific Ocean. J. Phys. Oceanogr. 18: 89-106.

Varadachari, V.V.R., Murty, C.S. and Das, P.K. (1968). On the level of least motion and the circulation in the upper layers of the Bay of Bengal. Bull. Nat. Inst. Sci. India, 38(Pt. I): 301-307.

Varkey, M.J. (1986). Salt balance and mixing in the Bay of Bengal. Ph.D. thesis (unpubl.), Kerala University, Kerala, India, 109 p.

Varkey, M.J. and Sastry, J.S. (1988). Reference depth for geostrophic computation - a new method. Indian J. Mar. Sci. 17: 91-93.

Wyrtki, K. (1971). Oceanographic atlas of International Indian Ocean Expedition. Nat. Sci. Found., Washington, D.C., 531 p.

Young, W.R. and Rhines, P.B. (1982). A theory of wind driven circulation. II. Gyres with western boundary layers. J. Mar. Res., 40: 849-872.